



## Film-based fluorescence sensing: a “chemical nose” for nicotine†

Cite this: *Chem. Commun.*, 2019, 55, 12679

Received 31st August 2019,  
Accepted 19th September 2019

DOI: 10.1039/c9cc06771j

rsc.li/chemcomm

Ke Liu, Jing Zhang, Ling Xu,  Jing Liu,  Liping Ding,  Taihong Liu \* and Yu Fang \*

**A novel series of emissive *o*-carborane derivatives, which showed multicolor, highly solid-state emission ( $\Phi_F \geq 43\%$ ) and ideal photochemical stability, were synthesized. Inspired by the powerful mammalian olfactory system, we, for the first time, successfully obtained a fluorescent sensor array, which exhibits superior detection capability for nicotine in the gaseous phase (down to 3 ppb). Furthermore, the sensor array can be extended to detect nicotine in aqueous solution at the nano-gram level ( $\sim 0.1 \text{ ng cm}^{-2}$ ) and determine the smoke of cigarette and electronic cigarette.**

According to the World Health Organization (WHO) report on the global tobacco epidemic, tobacco smoke killed at least 3.3 million people in 2017, and millions more suffer from lung cancer, tuberculosis, asthma or other chronic lung diseases caused by smoking.<sup>1</sup> A common view is that tobacco smoke contains more than 7000 chemicals (69 of which are known to cause cancer),<sup>2</sup> and is considered as a dangerous form of indoor air pollution, where nicotine is the most dangerous ingredient and the main reason for addiction. A number of countries have legislated against smoking by restricting cigarette advertising, regulating who can buy and use tobacco products, and even banning smoking in public areas.<sup>3</sup> Although GC-mass,<sup>4</sup> electrochemical methods,<sup>5</sup> surface enhanced Raman spectrometry,<sup>6</sup> chemiresistors,<sup>7</sup> and fiber optic sensors<sup>8</sup> have been developed to detect nicotine, there are no methods which can be used for the *in situ* detection or monitoring of nicotine vapor in public places since they must be robust, inexpensive, and have a rapid response, especially when there are large numbers of samples to process. The desire to detect and identify trace amounts of airborne analytes related to tobacco smoke with ever increasing sensitivity and selectivity continues to be one of the main drivers in sensor research.<sup>9</sup>

Key Laboratory of Applied Surface and Colloid Chemistry (Ministry of Education), School of Chemistry and Chemical Engineering, Shaanxi Normal University, Xi'an 710119, P. R. China. E-mail: liuth121@snnu.edu.cn, yfang@snnu.edu.cn

† Electronic supplementary information (ESI) available: Experimental procedures, characterization, crystallographic data and the sensing response. CCDC 1917767–1917770. For ESI and crystallographic data in CIF or other electronic format see DOI: 10.1039/c9cc06771j

Fluorescence provides a highly sensitive and selective method for quantification of a wide variety of analytes. Over the past decades, fluorescent-based sensors have been increasingly captivating the attention of scientists, and have appeared as one of the most promising candidates for chemical sensing.<sup>10</sup> In addition, due to their several unique advantages such as great design ability, outstanding sensitivity, re-usability and low cost, film-based fluorescent sensors have achieved great progress during the last few decades.<sup>11</sup> Suitable film-based fluorescent materials have to fulfill several important requirements: (1) high photochemical stability and high quantum yield in the solid state; (2) a fast and reversible sensing process; and (3) a simple preparation process and easy to be made into devices. Although a good deal of film-based fluorescent sensors exhibiting high sensing performances has been developed,<sup>12</sup> the photochemical stability and quantum yield in the solid state are often downplayed in practical use, which may explain why few sensors can be actually used.<sup>13</sup> Therefore, the development of fluorescent materials with superior photochemical stability and high quantum yield in the solid state is of great significance for developing high-performance film-based fluorescent sensors.

To construct fluorescent materials that possess superior photochemical stability in the solid state, we focused on a globular substituent called *o*-carborane. Unique *o*-carborane bears multiple properties such as a three-dimensional cage structure and intrinsic electron-deficient properties, and has been proven to be a promising building block for photo-functional materials.<sup>14</sup> In particular, its electron-withdrawing ability can lead to considerable charge redistribution in the luminescent core, which can further result in a large emission shift and better sensitivity to its chemical surroundings.<sup>15</sup> Recent studies showed that most of the *o*-carborane derivatives exhibited aggregation-induced emission (AIE) properties, when a  $\pi$ -conjugated aryl unit is connected to the C1 (and/or C2) position of *o*-carborane,<sup>16</sup> which means that the derivatives are fluorescence silent in the solution state, whereas they are recovered in the aggregated state owing to freezing the C1–C2 bond vibrations.<sup>17</sup> Therefore, *o*-carborane-based materials could

be one of the promising candidates for developing high-performance fluorescent film sensors.<sup>18</sup>

Meanwhile, by using the simultaneous interaction of multiple analytes with different sensing materials, the “chemical nose” is able to recognize the overall changes in the makeup of complex mixtures, rather than just identifying specific elements.<sup>19</sup> The data-rich outputs of array-based sensing methods are becoming much powerful and widely adopted by the analytical community, due to the improved capabilities with statistical and cheminformatic methods in the analysis process, as well as the recognition that many complex sensing challenges cannot be solved with conventional analytical tools. To get an *o*-carborane-based fluorescent sensor, herein, a new series of multicolor *o*-carborane-based fluorophores were designed, synthesized and further used for fabricating a film-based fluorescent sensor array. Four *o*-carborane derivatives demonstrated high fluorescence quantum yields and superior photochemical stability in the solid state. Interestingly, the array-based sensing platform is super-sensitive to nicotine and tobacco smoke. This communication reports the findings.

The four *o*-carborane-derived fluorophores (F1, F2, F3, and F4) were synthesized with high yields *via* a modified Pd-catalyzed Suzuki cross-coupling reaction (Scheme S1, ESI†). The details of the synthesis and characterization are provided in the ESI.† The crystal structures of the *o*-carborane derivatives were determined, and the results are shown in Fig. 1a. As seen from Fig. 1b, the compounds as created showed bright, different colors under UV light, varying from blue to red that covers almost the entire visible light region, which are probably due to the different donating abilities of the substituents. Casting the CHCl<sub>3</sub> solutions of the relevant compounds in routine filter papers (Whatman<sup>®</sup>, No GB/T1914-2007) resulted in four fluorescent films, which are respectively named Film 1, Film 2, Film 3 and Film 4, in the same order of the fluorophores (F1–F4). Again, the films are highly fluorescent as depicted in the figure. The observation may be ascribed to the hindrance from the rigid caging structure of the *o*-carborane unit, which is able to reduce concentration-related self-quenching owing to the prevention of intermolecular interactions.

To verify the statement, UV-vis absorption and photoluminescence spectra of the films were measured (Fig. S1a, ESI†). It is observed that with increasing electron-donating ability of the

substituents from hydrogen to dimethylamine, the absorption maxima bathochromically shifted from 300 nm to 307 nm, then to 312 nm, and finally to 334 nm for the films from 1 to 4. In contrast to the ground state absorption, the fluorescence emission maxima covered a wide range from 500 nm to 648 nm. In addition, Stokes' shift of the fluorophores F1–F4 increased from 200 nm of F1 to 314 nm of F4 with the same trend of the electron donating ability of the substituents. In addition, the four fluorophores as obtained showed high fluorescence quantum yields in the solid state with ~0.43 for F1, ~0.59 for F2, ~0.92 for F3, and ~0.58 for F4, respectively.

To provide an additional understanding of the optical properties, the highest occupied molecular orbitals (HOMOs) and the lowest unoccupied molecular orbitals (LUMOs) of the four fluorophores were calculated by using density functional theory (DFT) at the B3LYP/6-31G(d) level with the Gaussian 09 suit program. As provided in Table S1 (ESI†), the calculated energy levels of the HOMOs of the compounds gradually increased from -7.82 eV (F1) to -6.46 eV (F4), and the LUMOs increased from -0.262 eV (F1) to -0.049 eV (F4), confirming that the electron-donating ability of the substituent is capable of modifying the energy levels of the compounds. The large Stokes' shifts and strong emissions as demonstrated, no doubt, are in favour of sensing and device-making, owing to the reducing requirements for hard-wares and signal processing.

Since photochemical stability is a necessary requirement for practical applications of organic photo-materials, such as organic light emitting diodes (OLEDs), semiconductor lasers, fluorescent sensors, *etc.*<sup>20</sup> Therefore, we evaluated such properties of the compounds as created in the film state and the results are shown in Fig. S1b (ESI†). As observed, the fluorescence intensity of the films showed less than 4% decrease in 10 hours illumination, indicating that the compounds possess good stability towards air and light under ambient conditions, laying the foundation for long-term use. This property can be ascribed to the unique nonplanar structure of the *o*-carborane-based compounds as revealed by others.<sup>16</sup>

The single-crystals of the *o*-carborane derivatives as synthesized were obtained *via* controlled evaporation in their solutions in CH<sub>2</sub>Cl<sub>2</sub>/*n*-hexane. The crystal structures and the relevant crystallographic data are provided in Fig. 1a and Tables S2–S5 (ESI†). As seen, the benzene rings of the diphenyl units are nonplanar ascribing to the rotation of the C–C single bond in between, and the bond length of C1–C2 in the *o*-carborane unit of the compounds under examination changed from 1.721 Å to 1.729 Å, then to 1.731 Å, and finally to 1.732 Å for the four fluorophores from F1 to F4. This is a reasonable result as they are significantly longer than that of the unsubstituted *o*-carborane, 1.62 Å, as substitution will increase the length of the bond due to steric and electronic reasons.<sup>21</sup>

Based on the discoveries, it is anticipated that intermolecular interactions could be weakened in the crystal state due to the bulky icosahedral *o*-carborane structure. As seen from the structures depicted in Fig. 1a, there should not be any strong noncovalent interaction within the crystals of the *o*-carborane derivatives except F2 and F3, and the driving force for the crystallization could only

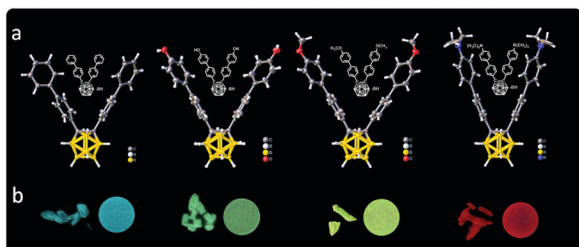


**Fig. 1** Structure and fluorescent pictures of the *o*-carborane-based fluorophores. (a) Crystal structures of fluorophores F1–F4, carbon (gray), boron (yellow), oxygen (red), nitrogen (blue) and hydrogen (white) atoms are shown as ellipsoids at a 50% probability level. (b) Relevant fluorescent photographs of the crystals and films under UV light.

come from the dispersion force, orientation force, induction force, *etc.* As seen from Fig. S2a (ESI<sup>†</sup>), the hydrogen bond does exist in the crystal of F2. As for F3, stronger Beage–H... $\pi$  (2.568 Å), C–H... $\pi$  (3.390 Å) and  $\pi$ ... $\pi$  (2.838 Å) interactions are observed (Fig. S2c, ESI<sup>†</sup>). It is the weak intermolecular interactions that make the compounds pack into the crystals as depicted in Fig. S2b and d (ESI<sup>†</sup>). With comparison of the structures of the two crystals, it is seen that F2 exists in a more regular structure and possesses rich channels, which is beneficial to chemical sensing due to a mass transfer reason.

Based on the aforementioned properties, a conceptual multicolor sensor array was constructed using the *o*-carborane-based fluorophores as sensing elements. All sensing tests related to evaluating the sensing performance of the individual compound-based films were conducted on a home-made, one-film device-based sensing platform.<sup>22</sup> In detail, a photodiode with maximum luminescence at  $\sim$ 310 nm was chosen as the light source for all the film-based devices. The measurements for different compound-based films were conducted by simply changing the photosensitive diodes, of which 500 nm for Film 1, 530 nm for Film 2, 545 nm for Film 3 and 650 nm for Film 4, respectively. The results are depicted in Fig. 2.

As seen, 9 chemicals with different properties were selected as representatives to conduct the tests, and the compound-based films exhibited different responses to the chemicals under examination in the vapor phase. Hot plots of the response intensities of the film-based devices to the chemicals resulted in easily distinguishable patterns as shown in Fig. 2a. To verify the reliability of the discrimination, a pattern recognition algorithm (PCA) was used to conduct additional analysis. The results are depicted in Fig. 2b. Clearly, the PCA score plot as generated shows clear clustering of the data using only the first two principle components, PC1 and PC2, where PC1 carries about 47.26% of the variance and PC2 carries 15.28%, demonstrating the strong discriminating capability of the *o*-carborane-based film devices. Fortunately, nicotine, one of the 9 chemicals under examination, can be identified with no difficulty from either of the two analysis methods.

The sensing performances of the sensing devices to nicotine were specially estimated owing to carcinogen reasons. Film 2 was chosen for conducting the specific analysis as it shows

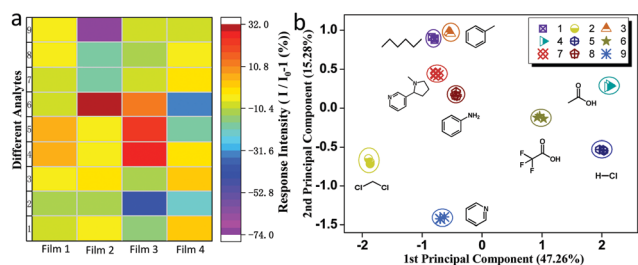


Fig. 2 Sensing performances of the multicolor sensor array. (a) Hot plot of the response intensity of the films on exposure to various analytes. (b) Two-dimensional PCA score plot for discriminating saturated vapor of the tested chemicals at 293 K via utilization of the response intensity of the sensor array.

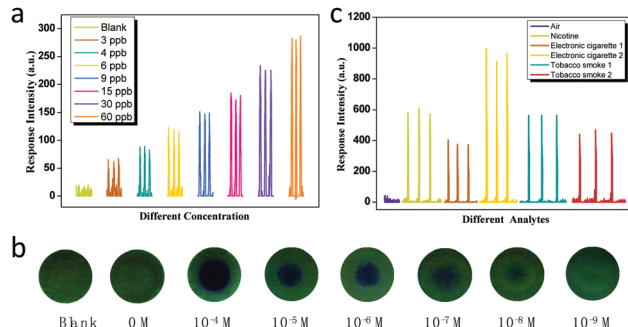


Fig. 3 Sensing performances of Film 2 to nicotine and tobacco smoke. (a) Net responses of different concentrations of nicotine vapor with the film-made device. (b) Photograph of the fluorescence quenching of Film 2 by nicotine on the contact mode (2  $\mu$ L of the nicotine with a spot area of  $\sim$ 0.2  $\text{cm}^2$ ) when viewed under 254 nm UV illumination. (c) Different response of nicotine, tobacco smoke and electronic cigarette.

more pronounced responses to the analyte (Fig. S3, ESI<sup>†</sup>), which is possibly a result of its unique adlayer structure related to the packing of the sensing fluorophore in the crystal state as depicted in Fig. S2a and b (ESI<sup>†</sup>). Furthermore, the presence of the hydroxyl groups in the sensing fluorophore may endow the film with an ability to enrich nicotine from the air through hydrogen bonding. To examine the performance, the detection limit (DL) of Film 2 to nicotine in the vapor phase was determined by collecting the response intensities in the presence of different concentrations of the chemical. As shown in Fig. 3a, the response intensity increased significantly upon increasing the concentration of the analyte. Even 3 ppb of nicotine vapor could result in a significant response to the film, suggesting that the DL is lower than the value.

Detection of extremely small amounts of nicotine in aqueous solution is also very important. To test this possibility, nicotine solutions of different concentrations were prepared and 2  $\mu$ L of each solution was piped on a routine test paper strip to receive a spot area of  $\sim$ 0.2  $\text{cm}^2$ . The visual fluorescence responses are shown in Fig. 3b. As seen, the minimum detectable amount by the naked eye is lower than 2  $\mu$ L of  $6.0 \times 10^{-8}$  mol  $\text{L}^{-1}$  solution, which is  $\sim$ 0.1 ng  $\text{cm}^{-2}$ , a value much lower than the results previously achieved using other detection methods (Table S6, ESI<sup>†</sup>).<sup>23</sup>

In order to mimic the real scenario, four kinds of tobacco smoke and electronic cigarette have also been tested using the same film-based device. The obtained results, depicted in Fig. 3c, show that 10 times dilution of their saturated vapors with air could still induce high response, suggesting the existence of gaseous nicotine. This is in support of the statement from WHO that electronic smoke could still lead to health problems and it cannot be taken as an effective method to quit smoking.<sup>3</sup> Humidity may also be an affecting factor to the tests, and thereby its effect on the sensing film's performance was investigated, and the results are shown in Fig. S4 (ESI<sup>†</sup>). As seen, the film's emission is hardly affected by water vapor. In addition, the film recovers much faster than that after detection of nicotine.

Reusability is an unavoidable factor to be considered if an analytical technique is to be used practically. For this reason,

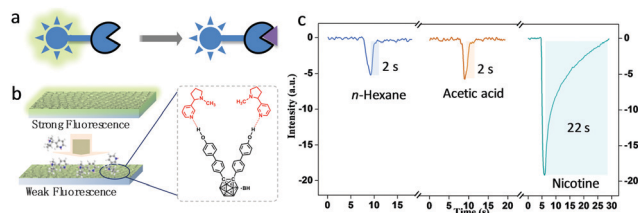


Fig. 4 Schematic representation of the sensing mechanism and dynamic responses of Film 2 to different analytes. (a) Schematic representation of typical fluorophore-receptor sensors for analytes; (b) probable interaction of nicotine with fluorophore F2; and (c) dynamic responses of Film 2 to the presence of different analytes in the vapor phase.

the reusability of the Film 2-based device to tobacco smoke was examined. Before testing, the saturated vapor from the smoke was diluted 10 times with air, and then tested with the device. As depicted in Fig. S5 (ESI<sup>†</sup>), the measurement lasted 5 days, and each day contained 10 independent tests. The result demonstrated that the sensing is fully reversible, and the device showed no distinct change in the sensing behaviour within 5 days, indicating that the film-based device has the potential to be developed into a portable fluorescent nicotine detector.

To understand the sensing performance of the film-based device, a possible sensing mechanism and some real time-dependent response traces to different chemicals are shown in Fig. 4. As aforementioned, *o*-carborane-based fluorophores F1–F4 are all aggregation-induced emitters (AIEgens) with bright emission in the solid state. As seen, the sensitive response of the Film 2-based device to nicotine could be understood by considering the possible hydrogen bond formation as shown, at the same time, it is the binding that may screen, at least partially, the packing of the F2 molecules within the film adlayer, resulting in decreased fluorescence emission. This binding may also explain why the fluorescence recovers 10 times slower in the sensing of this analyte than that of acetic acid or *n*-hexane (Fig. 4c). There is no doubt that the difference in the response dynamics can be used as an additional factor for the discrimination when it is necessary.<sup>24</sup>

In summary, we developed four *o*-carborane-based fluorophores which showed multicolour, high emission and photochemical stability in the solid state. The fluorophores as obtained were further employed for fabricating relevant fluorescent films and film-based devices. Additional studies demonstrated that the film-based devices showed discriminative responses to 9 representative chemicals including nicotine. Importantly, the device based on F2 showed unprecedented sensing capability to nicotine both in the vapor and aqueous solution with detection limits even lower than 3 ppb and 0.1 ng cm<sup>-2</sup>, respectively. More importantly, tobacco smoke and electronic cigarette can

be sensitively and selectively detected. We strongly believe that the Film 2-based device as obtained has the potential to be developed into a portable fluorescent nicotine detector.

This work was supported by the Natural Science Foundation of China (21527802, 21673133, and 21820102005), the 111 project (B14041), the Program for Changjiang Scholars and Innovative Research Team in University (IRT-14R33), the Natural Science Basic Research Program of Shaanxi (2019JM-404) and the Fundamental Research Funds for the Central Universities (GK201803024).

## Conflicts of interest

The authors declare no conflict of interest.

## Notes and references

- World Health Organization, WHO Report on the Global Tobacco Epidemic 2017, WHO Document Production Services, Geneva, Switzerland, 2018.
- U.S. Preventive Services Task Force, *Ann. Intern. Med.*, 2015, **163**, 622–634.
- M. Ernst, J. A. Matochik, S. J. Heishman, J. D. Vanhorn, P. H. Jons, J. E. Henningfield and E. D. London, *PANS*, 2001, **98**, 4728–4733.
- F. Baumann, R. Regenthal, I. L. Guerrero, U. Hegerl and R. Preiss, *J. Chromatogr. B*, 2010, **878**, 107–111.
- X. Q. Li, H. L. Zhao, L. B. Shi, X. Zhu, M. B. Lan, Q. Zhang and Z. H. Fan, *J. Electroanal. Chem.*, 2017, **784**, 77–84.
- N. Itoh and S. E. J. Bell, *Analyst*, 2017, **142**, 994–998.
- Y. Liu, S. A. Boampong, J. J. BelBruno, M. A. Crane and S. E. Tanski, *Nicotine Tob. Res.*, 2013, **15**, 1511–1518.
- R. Tabassum and B. D. Gupta, *Biosens. Bioelectron.*, 2017, **91**, 762–769.
- J. Fang, S. C. Park, L. Schlag, T. Stauden, J. Pezoldt and H. O. Jacobs, *Adv. Funct. Mater.*, 2014, **24**, 3706–3714.
- R. Pinalli, A. Pedrinia and E. Dalcanale, *Chem. Soc. Rev.*, 2018, **47**, 7006–7026.
- Y. Y. Qi, W. J. Xu, R. Kang, N. N. Ding, Y. L. Wang, G. He and Y. Fang, *Chem. Sci.*, 2018, **9**, 1892–1901.
- Y. Y. Fu, J. P. Yu, K. X. Wang, H. Liu, Y. G. Yu, A. Liu, X. Peng, Q. G. He, H. M. Cao and J. G. Cheng, *ACS Sens.*, 2018, **38**, 1445–1450.
- O. S. Wolfbeis, *Angew. Chem., Int. Ed.*, 2013, **52**, 9864–9865.
- D. Tu, P. Leong, S. Guo, H. Yan, C. Lu and Q. Zhao, *Angew. Chem., Int. Ed.*, 2017, **56**, 11370–11374.
- X. Li, X. Tong, Y. H. Yin, H. Yan, C. S. Lu, W. Huang and Q. Zhao, *Chem. Sci.*, 2017, **8**, 5930–5940.
- H. Naito, K. Nishino, Y. Morisaki, K. Tanaka and Y. Chujo, *J. Mater. Chem. C*, 2017, **5**, 10047–10054.
- K. Kokado and Y. Chujo, *Macromolecules*, 2009, **42**, 1418–1420.
- K. Liu, C. D. Shang, Z. L. Wang, Y. Y. Qi, R. Miao, K. Q. Liu, T. H. Liu and Y. Fang, *Nat. Commun.*, 2018, **9**, 1695.
- Z. Li and K. S. Suslick, *ACS Sens.*, 2018, **3**, 121–127.
- M. Schaferling, *Angew. Chem., Int. Ed.*, 2012, **51**, 3532–3554.
- M. Scholz and E. H. Hawkins, *Chem. Rev.*, 2011, **111**, 7035–7062.
- Z. L. Wang, K. Liu, X. M. Chang, Y. Y. Qi, C. D. Shang, T. H. Liu, J. Liu, L. P. Ding and Y. Fang, *ACS Appl. Mater. Interfaces*, 2018, **1041**, 35647–35655.
- B. Y. Lin, J. M. Chen, Y. B. Zeng, L. Li, B. Qiu, Z. Y. Lin and L. H. Guo, *ACS Sens.*, 2019, **4**, 1844–1850.
- R. A. Potyrailo, *Chem. Rev.*, 2016, **116**, 11877–11923.